Trajectory optimization of the 6-degrees-of-freedom high-speed parallel robot based on B-spline curve

Jiangping Mei🆔, Fan Zhang🆔, Jiawei Zang, Yanqin Zhao and Han Yan

Key Laboratory of Mechanism Theory and Equipment Design of the State
Ministry of Education, Tianjin University, Tianjin, China

Abstract

According to the problem that the existing high-speed parallel robot cannot satisfy the operation requirements of non-planar industrial production line, a 6-degrees-of-freedom high-speed parallel robot is proposed to carry out the kinematic and dynamic analyses. Combining with the door-type trajectory commonly used by the parallel robot, it adopts 3-, 5-, and 7-time B-spline curve motion law to conduct the trajectory planning in operation space. Taking the average cumulative effect of joint jerky as the optimization target, a trajectory optimization method is proposed to improve the smoothness of robot end-effector motion with the selected motion law. Furthermore, to solve the deformation problem of the horizontal motion stage of the trajectory, a mapping model between the control point subset of B-spline and the motion point subset of trajectory is established. Based on the main diagonally dominant characteristic of the coefficient matrix, the trajectory deformation evaluation index is constructed to optimize the smoothness and minimum deformation of the robot motion trajectory. Finally, compared to without the optimization, the maximum robot joint jerk decreases by 69.4% and 72.3%, respectively, and the maximum torque decreases by 51.4% and 38.9%, respectively, under a suitable trajectory deformation.

Keywords

Parallel robot, B-spline curve, robot modeling, trajectory planning method, optimization design

Introduction

High-speed parallel robots are widely used in industrial production lines, such as food industry, pharmaceutical industry, and electronics industry. They are mainly

Corresponding author:

Fan Zhang, Key Laboratory of Mechanism Theory and Equipment Design of the State Ministry of Education, Tianjin University, 135 Yaguan Road, Haihe Education Park, Jinnan District, Tianjin 300350, China.
Email: zf247@tju.edu.cn

used to complete high-speed sorting, packing, stacking, and assembly. However, the high-speed parallel robots with less degrees of freedom (DOF) cannot meet the complex industrial production requirements. Therefore, the application of 6-DOF high-speed parallel robots is gradually increasing. They have higher requirements for robot motion and hence should be optimized from the aspects of dynamics and trajectory planning to improve the smoothness of motion and inhibit the residual vibration of the robot.[1–3]

The trajectory planning method of the robot can be divided into two categories according to the space in which it is located, namely, joint space trajectory planning[4,5] and operating space trajectory planning.[6,7] The trajectory planning in joint space is based on the motion mapping relationship between the operation space and the joint space, and the corresponding motion position sequence of the joint is solved according to the key pose sequence of the end-effector trajectory, so it can achieve better motion smoothness. However, because the motion mapping relation between the joint space and the operating space is usually non-linear, it cannot guarantee that the end of the robot moves strictly according to the given trajectory. Hence, the trajectory planning in operating space is usually used in robot control and actual production.

In terms of the selection of the laws of motion, polynomial laws of motion, trapezoidal acceleration laws, sinusoidal laws of motion, and low-order spline laws are usually adopted.[8–10] At present, domestic and foreign scholars have conducted extensive research in this field. For example, Angeles et al.[11] proposed a method for the planning of operating space trajectories using piecewise polynomial functions. Macfarlane et al.[12] combined 5-time polynomial motion law and sinusoidal motion law and proposed a path planning method for robot. The method is connected by sinusoidal movement at the beginning and end of the trajectory, thus reducing the residual vibration at the end of the robot. Liu et al.,[13] based on the 7-time B-spline motion law, proposed a method to make the initial and final velocities, accelerations, and jerks of the robot joint freely configured at the same time. In terms of the research on the robot trajectory optimization method, Li et al.[14] planned the hyperactivity curve of the trajectory based on sinusoidal and linear motion laws and then obtained the modified s-shaped motion law. Based on the motion law of B-spline, Sencer et al.[15] considered the minimum trajectory motion error as the index to obtain the optimal motion trajectory. Rew and Kim[16] and Ha et al.[17] proposed the concept of the rate coefficient of sudden change of degree for the deceleration phase of the trajectory so as to construct an asymmetric s-curve movement rule for reducing the robot vibration.

In most of the above mentioned trajectory planning and optimization methods, the B-spline motion law is widely used in the actual process. Because, on the one hand, it can effectively reduce the motion parameters required by the robot, on the other hand, more than 5-time B-spline it can achieve the curve smoothness of the robot acceleration and jerk to reduce the vibration in the movement.[18–20] However, regarding parallel robot, the previous trajectory planning method based on high-order B-spline motion law is seldom studied. Especially when the parallel robot

moving platform has 6 DOF simultaneously in the working space, whether the B-spline motion law can meet the motion trajectory planning requirements of the robot joint space is still unclear. Hence, the relevant solution and analysis of the 6-DOF parallel trajectory planning method are necessary to be deepened in terms of the motion parameters and deformation error.

This article is organized as follows: Section "Kinematic analysis" introduces the 6-DOF high-speed parallel robot and builds the kinematic model of the parallel robot. In section "Dynamic analysis," according to the virtual work principle, the dynamic model of the parallel robot is illustrated. Section "Trajectory description" describes the pick-place trajectory curve commonly used by parallel robot in the production line. Section "The k time B-spline curve motion law" introduces the B-spline curve motion law and the computing method. Section "The trajectory planning in the joint space and the operating space," adopting 3-, 5- and 7-time B-spline curve motion law, simulates and analyzes the trajectory curve situation in the joint space and operation space. In section " The trajectory optimization in the operating space," according to the problems generated by the above procedure, an optimization method for 5- and 7-time B-spline curve is proposed. Finally, a summary and future prospects are detailed in section "Conclusion."

Kinematic analysis

The 6-DOF parallel robot is shown as in Figure 1, and it consists of a static platform, a moving platform, and six identical independent kinematic chains. Each kinematic chain is the RSS (R for revolute joint, S for spherical joint) construction, which has a motor, a reducer, a master arm, a slave arm, and two spherical joints. The master arm produces rotation movement driven by the motor. The slave arm is driven by the spherical joint mounted at the end of the active arm. The other end of the slave arm is connected to the moving platform. Through the six independent
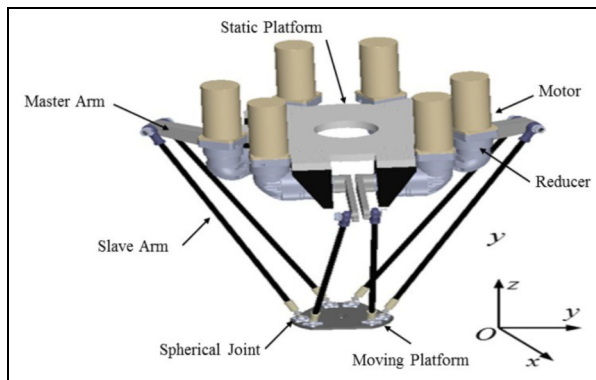

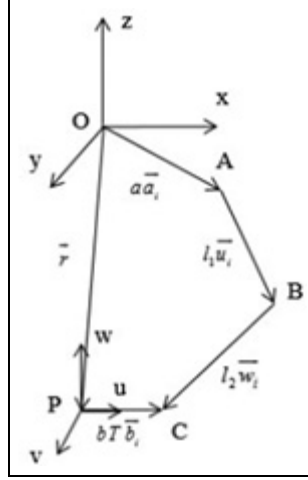**Figure 1.** The structure diagram of the 6-DOF parallel robot.

Figure 2. Vector diagram of a kinematic chain.

kinematic chains, the robot's moving platform can achieve 6 DOF in space, namely, three translational motions and three rotational motions.

Because the six kinematic chains have almost identical structures, the reference frame is defined as shown in Figure 2. The coordinate frame *O-xyz* is attached to the static platform, and the coordinate frame *P-uvw* is attached to the moving platform.[21] Therefore, the closed-loop position vector equation in the *i*th kinematic chain is expressed as

$$\vec{r} = a \cdot \vec{a_i} - T \cdot \overrightarrow{T_{bi}} + l_1 \cdot \vec{u_i} + l_2 \cdot \vec{w_i}, \quad i = 1-6 \tag{1}$$

where

$$\vec{r} = [x, y, z]^T$$
$$\vec{a_i} = [\cos(\phi_i), \sin(\phi_i), 0]^T$$
$$\overrightarrow{T_{bi}} = b \cdot [\cos(\varphi_i), \sin(\varphi_i), 0]^T$$
$$\vec{u_i} = [\cos(\phi_i)\cos(\theta_i), \sin(\phi_i)\cos(\theta_i), -\sin(\theta_i)]^T$$
$$T = R_\alpha R_\beta R_\gamma$$

The meaning of the kinematic parameters used in the above equation is illustrated in Table 1.

The inverse kinematics model can be obtained by equation (1), and the rotation angle of robot joint is shown as follows

$$\theta_i = 2\arctan \frac{-E_i - \sqrt{E_i^2 - G_i^2 + F_i^2}}{G_i - F_i} \tag{2}$$

Table 1. Meaning of the kinematic parameters.

Symbol	Meaning
$\vec{r}$	The direction vector from p to O in O-xyz
$\vec{a_i}$	The direction vector of static platform
a	The external circle radius of static platform
$\overrightarrow{T_{bi}}$	The product of direction vector and external circle radius of moving platform
$\vec{u_i}$	The product of direction vector and master arm
l_1	The length of the master arm
$\overrightarrow{w_i}$	The direction vector of the slave arm
l_2	The length of the slave arm
$\mathbf{T}$	The rotation matrix of the moving platform around three coordinate axes
α, β, γ	Euler angles of the moving platform around the x, y, and z axes

where

$$E_i = 2l_1(\vec{r} - a \cdot \vec{a_i} + \mathbf{T} \cdot \overrightarrow{T_{bi}})^T \hat{z}$$

$$F_i = -2l_1(\vec{r} - a \cdot \vec{a_i} + \mathbf{T} \cdot \overrightarrow{T_{bi}})^T (\cos \gamma_i \hat{x} + \sin \gamma_i \hat{y})$$

$$G_i = (\vec{r} - a \cdot \vec{a_i} + \mathbf{T} \cdot \overrightarrow{T_{bi}})^T (r - a \cdot \vec{a_i} + \mathbf{T} \cdot \overrightarrow{T_{bi}}) + l_1^2 - l_2^2$$

$$\vec{w_i} = (\vec{r} - a \cdot \vec{a_i} + \mathbf{T} \cdot \overrightarrow{T_{bi}} - l_1 \cdot \vec{u_i})/l_2$$

Taking the derivative of equation (1) with respect to time, the joint velocity equation can be obtained as follows

$$\dot{\boldsymbol{\theta}}_i = \frac{\overrightarrow{w_i}^T(\dot{\vec{r}} + \vec{\omega} \times \mathbf{T}\overrightarrow{T_{bi}})}{l_1 \vec{v_i}(\vec{u_i} \times \vec{w_i})}, \quad i = 1 - 6 \tag{3}$$

where $\dot{\vec{r}} = [\dot{x} \quad \dot{y} \quad \dot{z}]^T$ is the translational velocity of the moving platform, $\vec{\omega} = [\dot{\alpha} \quad \dot{\beta} \quad \dot{\gamma}]^T$ is the angular velocity of the moving platform, and $\vec{v_i} = (-\sin(\theta_i), \cos(\theta_i), 0)^T$ is the unit vector of the rotational axis of the ith proximal link, which is normal to the plane spanned by $\vec{a_i}$ and $\vec{u_i}$.

Equation (3) can be rewritten as follows

$$\dot{\boldsymbol{\theta}}_i = \mathbf{J} \cdot \dot{\boldsymbol{x}}; \quad \dot{\boldsymbol{x}} = [\dot{x} \quad \dot{y} \quad \dot{z} \quad \dot{\alpha} \quad \dot{\beta} \quad \dot{\gamma}]^T \tag{4}$$

where

$$\mathbf{J}_q = diag[l_1 \overrightarrow{w_i}^T (\vec{v_i} \times \vec{u_i})]$$

$$\mathbf{J}_1 = \begin{bmatrix} I_3 & T'_\alpha \overrightarrow{T_{bi}} & T'_\beta \overrightarrow{T_{bi}} & T'_\gamma \overrightarrow{T_{bi}} \end{bmatrix}_{18*6}$$

$$J_2 = \begin{bmatrix} \overrightarrow{w_1} & \mathbf{0}_{1*3} & \cdots & \cdots & \cdots & \mathbf{0}_{1*3} \\ \mathbf{0}_{1*3} & \overrightarrow{w_2} & \cdots & \cdots & \cdots & \mathbf{0}_{1*3} \\ \mathbf{0}_{1*3} & & \overrightarrow{w_3} & \mathbf{0}_{1*3} & \cdots & \mathbf{0}_{1*3} \\ \vdots & \cdots & \cdots & \overrightarrow{w_4} & \cdots & \mathbf{0}_{1*3} \\ \vdots & \cdots & \cdots & \cdots & \overrightarrow{w_5} & \mathbf{0}_{1*3} \\ \mathbf{0}_{1*3} & \cdots & \cdots & \cdots & \cdots & \overrightarrow{w_6} \end{bmatrix}_{6*18}$$

$$J_x = J_2 \cdot J_1$$

$$J = J_q^{-1} \cdot J_x$$

Jacobian matrix J reflects the mapping relation of the robot joint and end-effector, which is composed of direct Jacobian matrix J_q and indirect Jacobian matrix J_x. $\dot{x}$ is the velocity matrix of the robot end-effector.

Taking the quadratic derivative of equation (1) with respect to time, the joint acceleration equation can be obtained as follows

$$\ddot{\theta} = J \cdot \ddot{x} + F(\dot{r}); \quad \ddot{x} = \begin{bmatrix} \ddot{x} & \ddot{y} & \ddot{z} & \ddot{\alpha} & \ddot{\beta} & \ddot{\gamma} \end{bmatrix}^T \tag{5}$$

where $F(\dot{r})$ is the non-linear velocity term and $\ddot{x}$ is the acceleration matrix of the robot end-effector.

Taking the third derivative of equation (1) with respect to time, the joint jerk equation can be obtained as follows

$$\dddot{\theta} = J \cdot \dddot{x} + K(\dot{r}, \ddot{r})$$
$$\dddot{x} = \begin{bmatrix} \dddot{x} & \dddot{y} & \dddot{z} & \dddot{\alpha} & \dddot{\beta} & \dddot{\gamma} \end{bmatrix}^T \tag{6}$$

where $K(\dot{r}, \ddot{r})$ is the non-linear velocity and acceleration term and $\dddot{x}$ is the jerk matrix of the robot end-effector.

Dynamic analysis

Since the motion branch chain of the 6-DOF parallel robot is controlled independently, the local coordinate system O_i-$x_iy_iz_i$ on each chain should be established when building the dynamic model. The origin O_i of the local coordinate system is at the center of mass of the slave arm, the z_i axis always points to the axis direction of the slave arm, the x_i axis is located in the plane formed by $\vec{w_i}$ and $\vec{w_i} \times \vec{u_i}$, and the y_i axis is generated according to the right-handed rectangular coordinate system rule.

According to the virtual work principle and ignoring the friction, the dynamic equation of the parallel robot can be obtained as follows

$$\tau = \tau_a + \tau_v + \tau_g + \tau_{rod} \tag{7}$$

where

Table 2. Meaning of the dynamic parameters.

Symbol	Meaning
$\tau = \begin{pmatrix} \tau_1 & \tau_2 & \tau_3 & \tau_4 & \tau_5 & \tau_6 \end{pmatrix}^T$	The torque of robot joint
$m' = m_{platform} + m_{load}$	The mass of the moving platform
I_x, I_y, I_z	The inertia of the moving platform
η_{gear}, I_{gear}	The reduction ratio and inertia of gear
$f_{si} = m_{rod} \cdot \vec{r}_{di} + m_{rod} \cdot g\vec{z}$	The sum of inertial force and gravity of the slave arm
$m_{rod}, \vec{r}_{di}$	The mass and acceleration of the slave arm
$M_{rodi} = I_{rodi} \cdot \dot{\omega}_i$	The moment of inertia of the slave arm
$I_{rodi} = RI_{rod}R^T$	The inertia tensor of the slave arm relative to a fixed coordinate system
$I_{rod}, \dot{\omega}_i$	The inertia and angular acceleration of the slave arm

$$\boldsymbol{\tau}_a = I_A \boldsymbol{J} \cdot \ddot{\boldsymbol{x}} + \boldsymbol{J}^{-T}[m' \quad I_x\ddot{\theta}_x \quad I_y\ddot{\theta}_y \quad I_z\ddot{\theta}_z]$$

$$\boldsymbol{\tau}_v = I_A \cdot \boldsymbol{F}(\dot{\boldsymbol{r}}), I_A = I_{arm} + n_{gear}^2 I_{gearbox}$$

$$\boldsymbol{\tau}_{g1} = \boldsymbol{J}^{-T}[m'g\vec{z} \quad 0 \quad 0 \quad 0]^T$$
$$\boldsymbol{\tau}_{g2} = m_{arm}r_{arm}g[\cos\theta_1 \quad \dots \quad \cos\theta_6]^T$$

$$\boldsymbol{\tau}_g = \boldsymbol{\tau}_{g1} + \boldsymbol{\tau}_{g2}$$

$$\boldsymbol{\tau}_{rod} = \boldsymbol{J}^{-T} \sum_{i=1}^{6} (\boldsymbol{J}_{wi} \cdot M_{rodi} + \boldsymbol{J}_{vi} \cdot f_{si})$$

where $\boldsymbol{\tau}_a$ is the inertia torque component, $\boldsymbol{\tau}_v$ is the velocity torque component, $\boldsymbol{\tau}_g$ is the gravity torque component, and $\boldsymbol{\tau}_{rod}$ is the comprehensive torque component of the slave arm.

The meaning of the dynamic parameters used in the above equation is illustrated in Table 2.

Trajectory description

As the 6-DOF parallel robot is mainly used to complete the grasping and placing operations in practical engineering (Figure 3(a)), the typical motion mode of the end movement platform in the working space is point-to-point (PTP) motion, and it requires some certain obstacle avoidance points. And the specified motion trajectory of the parallel robot in the working space is shown in Figure 3(b). O_w-$x_wy_wz_w$ is the local coordinate system that the coordinate O-xyz translates $(H + h) - h_d$ along the negative direction of the z axis, and the parameters of the trajectory are defined in Table 3. Hence, the robot motion trajectory is a "door" type including
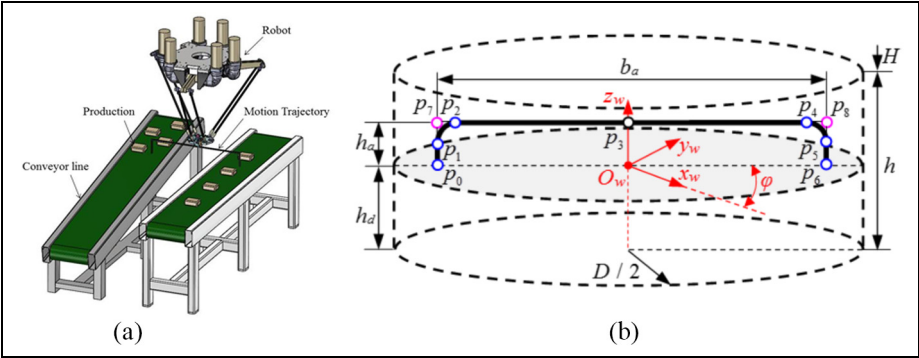
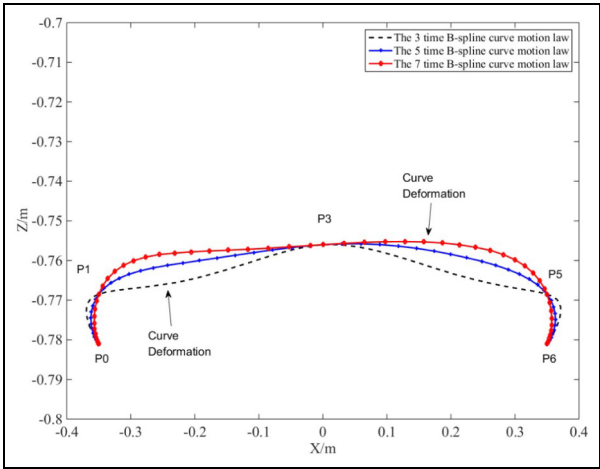**Figure 3.** Schematic of the motion trajectory in workspace.

Figure 4. The trajectory curve of different B-spline curve motion laws in the joint space without the rotation angle of the moving platform.

Table 3. Meaning of the trajectory curve parameters.

Symbol	Meaning
H	The distance from the static platform to the upper surface of the workspace
h	The height of the workspace
h_d	The height of the trajectory relative to the bottom surface of the workspace
h_a	The vertical height of the trajectory
b_a	The horizontal distance of the trajectory
φ	The angle of the trajectory relative to the local coordinate system.

Table 4. The random angle of the moving platform round the three axes.

	p_0	p_1	p_3	p_5	p_6
α	$-20°$	$5°$	$-10°$	$-20°$	$10°$
β	$25°$	$-10°$	$-20°$	$-15°$	$5°$
γ	$-5°$	$-25°$	$10°$	$-10°$	$20°$

the rising section p_0-p_7, the horizontal section p_7-p_8 (the central point of the horizontal section is p_3), and the descending section p_8-p_6.

In order to make the trajectory more compliant and reduce the impact and time consumption of the inflection on the robot motion, the mixed movement sections p_1-p_2 and p_4-p_5 are established. In addition, the standard trajectory adopted has an h_a of 0.025 m and b_a of 0.7 m. The maximum movement velocity of the robot is 120 times/min, so the optimal trajectory time is 0.25 s.

In addition, the randomly set rotation angles of the moving platform are added when the robot moves along the trajectory to verify the impact of the rotation angles of the dynamic platform on the trajectory planning. Since the specified moving platform does not rotate more than $\pm 30°$ around the three coordinate axes, the random rotation angle can be set as shown in Table 4.

The *k*-time B-spline curve motion law

For the robot trajectory curves to maintain smoothness, the *k*-time B-spline curve motion law is adopted in this article. According to the above trajectory description,[22] it selects the five key points, including p_0, p_1, p_3, p_5, and p_6, to obtain the five-group point-time series $\{p_i, t_i\}$ of the 6-DOF parallel robot.

First, $U = [u_0, u_1, \ldots, u_{n+2k}]$ is the domain node vector of the *k*-time B-spline curve, and n represents the number of key points. Using the accumulated chord length parametric method makes the time node normalized, which is shown below

$$
\begin{cases}
u_0 = u_1 = \cdots = u_k = 0 \\
u_{n+k} = u_{n+k+1} = \cdots = u_{n+2k} = 1 \\
u_i = u_{i-1} + \dfrac{|\Delta t_{i-k-1}|}{\sum\limits_{j=0}^{n-1} |\Delta t_j|} \quad i = k+1, \ldots, n+k-1
\end{cases} \tag{8}
$$

$$\Delta t_i = t_{i+1} - t_i$$

Second, $N_{i,k}(u)(i = 0, 1, \ldots, n)$ is the basis function of the *k*-time B-spline curve, which is shown below

$$\begin{cases} N_{i,0}(u) = \begin{cases} 1 & u_i < u < u_{i+1} \\ 0 & Othervise \end{cases} \\ N_{i,k}(u) = \dfrac{u - u_i}{u_{i+1} - u_i} N_{i,k-1}(u) + \dfrac{u_{i+k+1} - u}{u_{i+k+1} - u_{i+1}} N_{i+1,k-1}(u) \\ make\dfrac{0}{0} = 0 \end{cases} \tag{9}$$

Third, the B-spline curve equation can be shown as follows

$$p(u) = \sum_{i=0}^{n} d_i \cdot N_{i,k}(u) \tag{10}$$

where $d_i(i = 0, 1, \ldots, n)$ is the control vertices, and according to the DeBoor-Cox recursion formula,[23] it can be shown as

$$p(u) = \sum_{j=i-k+l}^{i} d_j^l \cdot N_{j,k-l}(u) = \cdots = d_i^k, u_i < u < u_{i+1}$$

$$d_j^l = \begin{cases} d_j & l = 0 \\ (1 - \alpha_j^l) \cdot d_{j-1}^{l-1} + \alpha_j^l \cdot d_j^{l-1} & \begin{matrix} l = 1, 2, \ldots, k \\ j = i - k + l, \ldots, i \end{matrix} \end{cases} \tag{11}$$

$$\alpha_j^l = \dfrac{u - u_j}{u_{j+k+1-l} - u_j}$$

where the r derivative equation of $p(u)$ is calculated as follows

$$p^r(u) = \sum_{j=i-k+l}^{i} d_j^r \cdot N_{j,k-r}(u), \quad u_i < u < u_{i+1}$$

$$d_j^l = \begin{cases} d_j & l = 0 \\ (k+1-l) \cdot \dfrac{d_j^{l-1} - d_{j-1}^{l-1}}{u_{j+k+1-l} - u_j} & \begin{matrix} l = 1, 2, \ldots, k \\ j = i - k + l, \ldots, i \end{matrix} \end{cases} \tag{12}$$

Fourth, the control vertices should be solved first, and the solution equation set is shown as follows

$$\boldsymbol{C_N} \cdot \boldsymbol{d} = \boldsymbol{p} \tag{13}$$

where $\boldsymbol{d}$ is the control vertices matrix, $\boldsymbol{C_N}$ is the coefficient matrix, and $\boldsymbol{p}$ is the motion parameter matrix. For example, using the 7-time B-spline curve motion law, the above matrix can be shown as

$$\boldsymbol{d} = \begin{bmatrix} d_0 & d_1 & \cdots & d_n & d_{n+1} & \cdots & d_{n+6} \end{bmatrix}^T \tag{14}$$

$$\boldsymbol{p} = \begin{bmatrix} p_0 & p_1 & \cdots & p_n & w_s & w_e & a_s & a_e & j_s & j_e \end{bmatrix}^T \tag{15}$$

where p_0 to p_n are the joint points that correspond to the key waypoints; w_s and w_e are the velocity of the start and end points, respectively; a_s and a_e are the acceleration of the start and end points, respectively; and j_s and j_e are the jerk of the start and end points, respectively. According to the parallel robot motion characteristic, the initial motion condition is set as

$$\begin{matrix} w_s = 0, & w_e = 0 \\ a_s = 0, & a_e = 0 \\ j_s = 0, & j_e = 0 \end{matrix} \tag{16}$$

Fifth, for the k-time B-spline curve, it must also increase $k - 1$ boundary conditions, which can be obtained by tangent vector boundary conditions. Due to the repeat times k on both ends, the k-time B-spline curve at the end of the first control vertex is at the end of the first data point, so the following $k - 1$ boundary conditions can be obtained

$$\begin{cases} p'_0 = p'(u_k) = d_1^1 = k \dfrac{d_1 - d_0}{u_{k+1} - u_1} \\ p'_n = p'(u_{n+k}) = d_{n+k-1}^1 = k \dfrac{d_{n+k-1} - d_{n+k-2}}{d_{n+2k-1} - d_{n+k-1}} \\ p''_0 = p''(u_k) = d_2^2 \\ p''_n = p''(u_{n+k}) = d_{n+k-1}^2 \\ p'''_0 = p'''(u_n) = d_3^3 \\ p'''_n = p'''(u_{n+k}) = d_{n+k-1}^3 \end{cases} \tag{17}$$

Finally, according to equations (8) and (9), the basis function can be calculated, and through equations (11) and (12), the control vertices can be obtained. Therefore, the position, velocity, acceleration, and jerk of the robot end-effector can be calculated using the B-spline curve equation (13). Then, through the kinematic inverse solution, the motion parameters of the robot joint can be obtained and a similar trajectory can be implemented.

The trajectory planning in the joint space and the operating space

In the joint space, by adopting the B-spline curve motion law, the trajectory curves of the robot end-effector without the rotation motion of the moving platform are shown in Figure 4. It shows that for different B-spline curve motion laws, although each trajectory can strictly pass the given trajectory points, there are slight differences between the trajectories, among which the maximum error of each trajectory in the direction of the extension z axis is about 9.4 mm. Meanwhile, as trajectory planning in joint space relies on the kinematic forward solution, the process to calculate the position is non-linear. Therefore, it will lead to deformation of robot end trajectory curve, which will have certain influence on robot motion.
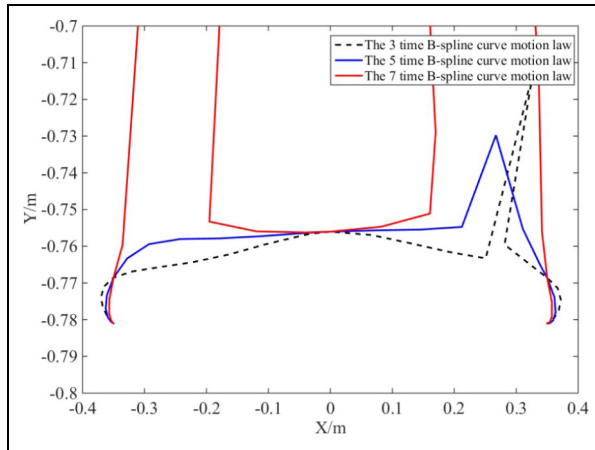
Figure 5. The trajectory curve of different B-spline curve motion laws in the joint space with the random rotation angle of the moving platform.

In addition, when the moving platform produces rotation motion, the trajectory curves of different B-spline curve motion laws in joint space are shown in Figure 5. Then, when the robot end-effector produces arbitrary angular motion, the non-linear effect will aggravate the deformation of the movement curve of the robot end-effector and produce irregular path changes. In the actual operation process, this situation will easily lead to the random motion of the robot, which will cause danger to the operation and easily bring about damage to the equipment. Hence, for the multi-DOF parallel robot, the B-spline curve motion rule is not suitable for the trajectory planning in the joint space.

In the operating space, by adopting the above motion analysis method, the motion law of different B-spline curves can be obtained, as shown in Figure 6. It shows that the trajectory curve of the different motion laws is similar. It can also strictly provide trajectory points p_0, p_1, p_3, p_5, and p_6, and there is no excessive deformation in the curve.

Figure 7 shows that the motion parameters of arbitrary robot active joints are compared and analyzed with different B-spline curve motion laws in workspace. According to Figure 7(a) and (b), the velocity curves of the robot active joint 1 are continuous and smooth with every motion law, but when adopting the 3-time B-spline curve, the starting acceleration of the robot active joint 1 is not equal to 0, the acceleration curve is not smooth, and there exists break point, thus implying that the driving torque provided by the joint motor as shown in Figure 7(d) does not guarantee complete smoothness, and there are sharp points that cause the robot jitter during motion, and the initial acceleration is not equal to 0. In addition, it can be clearly seen that when the 5-time B-spline curve motion law is adopted, the output torque demand provided by the motor is relatively small, reducing the motor consumption.
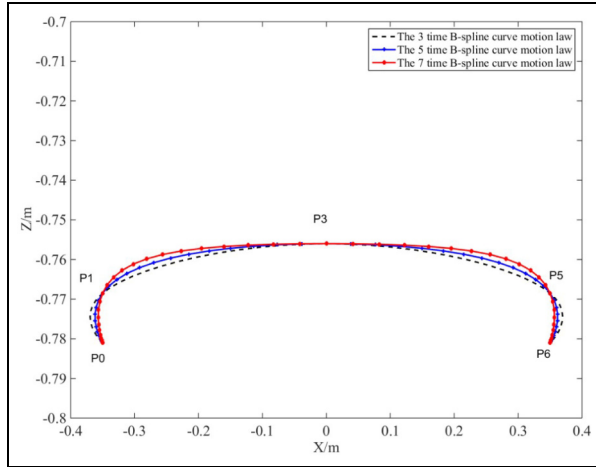
Figure 6. The trajectory curve of different B-spline curve motion laws in the workspace without and with the random rotation angle of the moving platform.

According to Figures 7(c) and 8, the 5- and 7-time B-spline curve motion law can guarantee the smoothness of jerk curve of the robot joint and end-effector. From these figures, only the jerk curve of the latter can be equal to 0 at start and end points so as to improve the motion stability of robot in the rapid picking and placing motion. However, no matter the joint or the end-effector, the maximum jerk value of the 5-time B-spline curve is less than the 7-time B-spline curve.

In addition, when the robot end-effector produces arbitrary angular motion, the motion curve of the robot end-effector will not be deformed like the joint space trajectory planning, so the workspace trajectory planning is applicable to the 6-DOF high-speed parallel robot, and the 5- or 7-time B-spline curve motion law can be given priority.

The trajectory optimization in the operating space

When performing tasks, robots are usually required to move as fast as possible. However, as the speed of motion increases, the acceleration and jerkiness are usually increased, which is not conducive to the smoothness and accuracy of the motion process. Therefore, it is necessary to optimize the motion track.

As the smoothness of the trajectory is mainly reflected in the value of jerkiness, it is necessary to ensure that it is not too large in the process of robot motion. Therefore, considering the average cumulative effect of the trajectory jerkiness in the process of motion, the following indexes can be defined to evaluate the smoothness of the trajectory
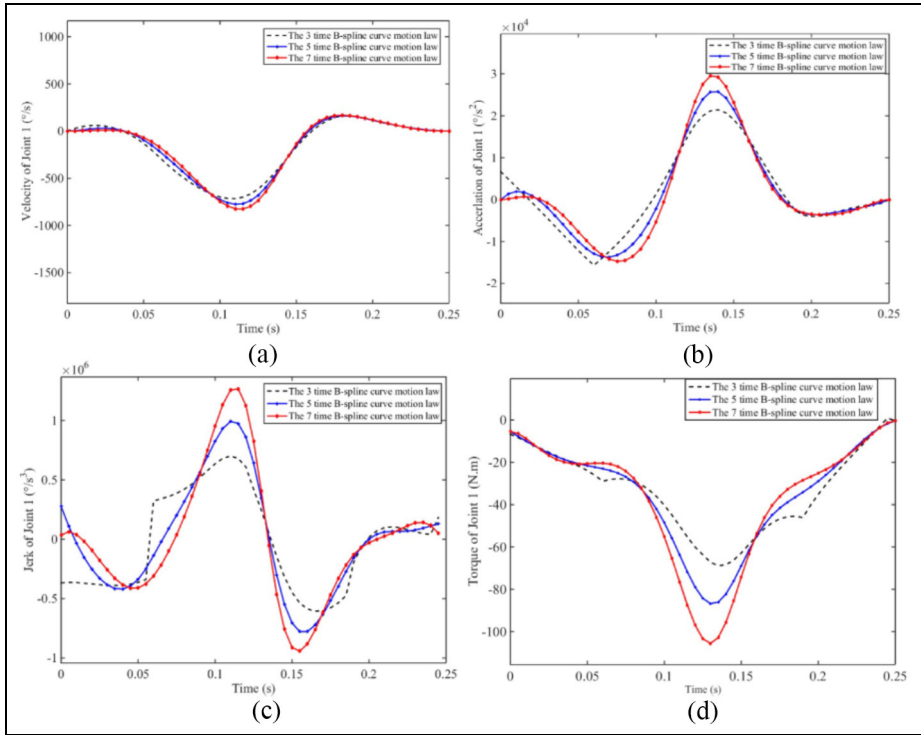
Figure 7. Comparison motion parameters of the robot joint with different motion laws in workspace: (a) velocity of robot joint 1, (b) acceleration of robot joint 1, (c) jerk of robot joint 1, and (d) torque of robot joint 1.
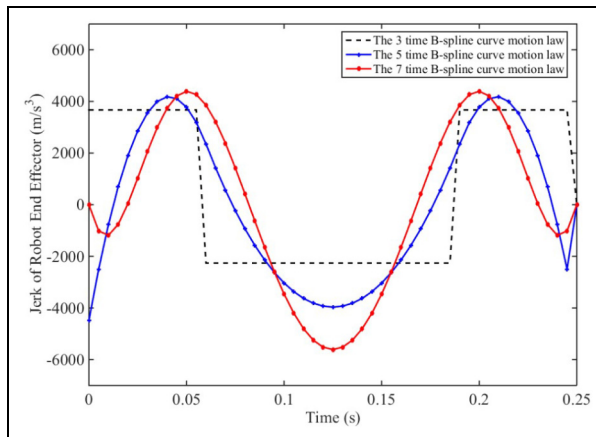

Figure 8. Comparison jerk curve of the robot end-effector with different motion laws in workspace.
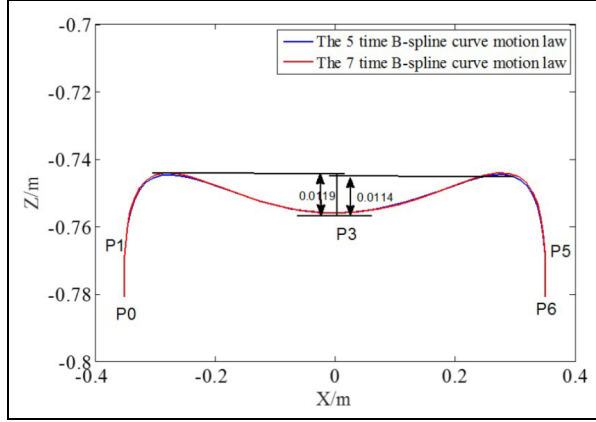
Figure 9. The trajectory after minimum jerk optimization.

$$\kappa_{jerk} = \sqrt{\frac{1}{n}\sum_{i=1}^{n}\int_{0}^{T_{total}}(j_i)^2\, d_t} \tag{18}$$

where n is the number of the robot joint and T_{total} is the total motion time. The optimization model of the trajectory can be shown as follows

$$\kappa_{jerk} \rightarrow min$$
$$s.t. \quad 2(T_1 + T_2) = T_{total}$$
$$\theta_{min} - \min_{i\in[1,\,n]}(\theta_i) \leq 0, \quad \max_{i\in[1,\,n]}(\theta_i) - \theta_{max} \leq 0 \tag{19}$$
$$\alpha \in [\alpha_{min}, \alpha_{max}], \ \beta \in [\beta_{min}, \beta_{max}], \ \gamma \in [\gamma_{min}, \gamma_{max}]$$

$$\max_{i\in[1,\,n]}(|\,v_i\,|) - v_{Mi,max}/\eta_{gear} \leq 0, \ |\,a_i\,| - a_{i,max} \leq 0, \ |\,\tau_i\,| - \tau_{i,max} \leq 0$$

where θ_{min} and θ_{max} are the maximum and minimum range of the robot joint rotation angle, respectively. $v_{Mi,max}$, $a_{i,max}$, and $\tau_{i,max}$ are the maximum values of the velocity, acceleration, and torque of the robot joint, respectively. Hence, adopting the 5- and 7-time B-spline curve motion law, the result of the optimization model is shown in Figure 9. It shows that the trajectory produces deformation after the minimum jerk optimization model, especially along the z-axis direction.

Table 5 compares the motion parameters of robot joints before and after optimization, and it can clearly see that using the minimum jerk method can effectively reduce the maximum speed, maximum acceleration, maximum jerk, and maximum input torque of the robot joints. In particular, after the optimization, the maximum jerk of the 5- and 7-time B-spline curves is $5.48 \times 10^{6\circ}/s^3$ and $4.25 \times 10^{6\circ}/s^3$, respectively, which is 66.4% and 77.3% lower than the maximum jerk of the previous trajectories. And the input torques of robot joints are also reduced by 36.4% and

Table 5. Comparison the motion parameters of the robot joint without optimization and after minimum jerk optimization.

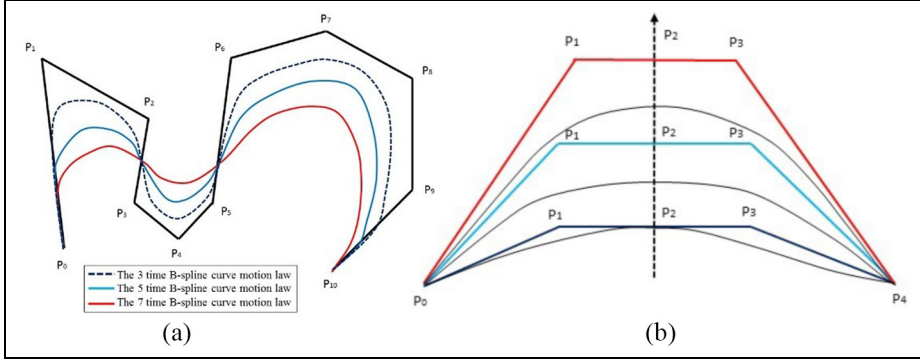|	Motion law	T_1 (s)	T_2 (s)	max $|v|$ (°/s)	max $|a|$ (°/s^2)	max $|j|$ (°/s^3)	max $|\tau|$ (N m)
No optimization	5-time B-spline	0.06	0.065	2.76×10^3	2.32×10^5	1.63×10^7	97.89
	7-time B-spline	0.06	0.065	2.74×10^3	1.89×10^5	1.87×10^7	103.37
Optimization with the minimum jerk	5-time B-spline	0.028	0.097	1.73×10^3	7.76×10^4	5.48×10^6	35.62
	7-time B-spline	0.037	0.088	1.89×10^3	7.74×10^4	4.25×10^6	38.84

Figure 10. The properties of B-spline curve: (a) closeness of curve to control vertex and (b) impact of control points on curve.

37.6%. Thus, the minimum jerk optimization model can obviously reduce the joint consumption during the movement of the robot and improve the smoothness of the trajectory.

However, no matter the 5- or 7-time B-spline curve motion law, the above optimization method can cause the deformation of the trajectory curve, where the maximum displacement from the trajectory's highest point to the given trajectory point P_3 is 11.4 and 11.9 mm. Hence, it is necessary to analyze the deformation cause of the B-spline curve.

According to the characteristics of the B-spline curve in Figure 10, on the one hand, with the higher order of the spline curve, the generated curve will deviate from its control vertex, as shown in Figure 10(a); on the other hand, when the intermediate control vertex deviates from the start and end points, the distance between the B-spline curve and the control vertex will be longer, as shown in Figure 10(b). Hence, relative to the 3-time B spline curve, when 5- or 7-time B spline curve is adopted to construct the motion trajectory, it is necessary to pay attention to the deformation of the motion trajectory.

Equation (13) can be rewritten as follows

$$d = (C_N)^{-1} \cdot p \tag{20}$$

which means that when the trajectory points d and trajectory motion parameters p are confirmed, the control vertex of the B-spline curve is decided by the matrix $(C_N)^{-1}$, which is confirmed by the time allocation method of the key points.

For the k-time B-spline motion law, if the repeatability of both nodes of the node vector U is set as $\varepsilon_d = k + 1$, then the control vertex number of the B-spline curve is $n + k$ according to the given trajectory $\{p_0, p_1, \ldots, p_n\}$. Thus, the matrix $(C_N)^{-1}$ is $n + k$-time square matrix. When the velocity, acceleration, and jerk of the starting and end points are equal to 0 along each direction, the control vertex matrix of the trajectory curve can be rewritten in the following form

$$
\begin{bmatrix} d_0 \\ d_1 \\ \vdots \\ \vdots \\ d_{n+k-1} \\ d_{n+k} \end{bmatrix} = \begin{bmatrix} c_{11} & \cdots & \cdots & c_{1(n+k-1)} & c_{1(n+k)} \\ c_{21} & \cdots & \cdots & c_{2(n+k-1)} & c_{2(n+k)} \\ \vdots & & & \vdots & \vdots \\ \vdots & & & \vdots & \vdots \\ c_{(n+k-1)1} & \cdots & \cdots & c_{(n+k-1)(n+k-1)} & c_{(n+k-1)(n+k)} \\ c_{(n+k)1} & \cdots & \cdots & c_{(n+k)(n+k-1)} & c_{(n+k)(n+k)} \end{bmatrix} \begin{bmatrix} p_0 \\ \vdots \\ p_n \\ 0 \\ \vdots \\ 0 \end{bmatrix} \quad (21)
$$

According to the calculation rule of matrix, when calculating the control vertex of k-time B spline trajectory, given the must-pass point sequence $\{p_0, p_1, \ldots, p_n\}$, the coefficient matrix $(C_N)^{-1}$ is equivalent to produce the linear influence on the must-pass point. For example, when calculating the control vertex d_0, all the other items except the calculation result of the diagonal element of the coefficient matrix $(C_N)^{-1}{}_{11} \times p_0$ are disturbance item, which makes the control vertex d_0 produce large displacement deviation and affects the shape of the curve. Therefore, combined with the theory of dominant diagonal of matrix, the main diagonal elements of matrix $(C_N)^{-1}$ and the elements of the other row and column satisfy the following inequality

$$
\forall p \in W, \quad \exists \kappa_i = |C_{ii}| - \sum_{i=1}^{n+k} \sum_{j=1, j\neq i}^{n+k} |C_{ij}| > 0 \quad (22)
$$

which means that κ_i reflects the coupling characteristics between the ith must-pass point and the rest must-pass points. The larger the κ_i, the smaller the influence of this coupling property on the curve shape, and the closer the control vertex is to its must-pass point. However, previous researchers used this property of the matrix to analyze the inertia matrix of the robot and defined the coupling characteristics between joints, but it is only used for the effective inertia of the single joint itself, without considering the influence between joints.[24] According to equation (22), the following indexes can be defined to reflect the influence of other must-pass points on the coupling characteristics of control vertices

$$
\kappa_1 = \frac{\displaystyle\sum_{i=1}^{n+k} \sum_{j=1, j\neq i}^{n+k} |C_{ij}|}{\displaystyle\sum_{i=1}^{n+k} |C_{ii}|} \quad (23)
$$

which indicates that if the effect of the coupling property between the must-pass points needs to be reduced, then the elements beside the main diagonal elements should be set to 0, or when C_{ij} is a fixed value, C_{ii} needs to be maximum and then the index κ_1 tends to be 0.

The eigenvalue analysis of matrix $(C_N)^{-1}$ can be obtained as follows

$$(C_N)^{-1} = Qdiag(\lambda_1, \lambda_2, \ldots, \lambda_{n+k})Q^{-1} =$$

$$\begin{bmatrix} q_1 & q_2 & \cdots & q_{n+k} \end{bmatrix} \begin{bmatrix} \lambda_1 & & & \\ & \lambda_2 & & \\ & & \ddots & \\ & & & \lambda_{n+k} \end{bmatrix} \begin{bmatrix} q_1^T \\ q_2^T \\ \vdots \\ q_{n+k}^T \end{bmatrix} \tag{24}$$

where λ_i is the eigenvalue of the matrix $(C_N)^{-1}$, q_i is the eigenvector for the corresponding λ_i, and Q is the orthogonal matrix, which is $Q^{-1} = Q^T$. Meanwhile, the matrix $(C_N)^{-1}$ can be decomposed into the following two submatrices

$$A = \begin{bmatrix} 0 & c_{12} & \cdots & c_{1(n+k)} \\ c_{21} & 0 & \cdots & c_{2(n+k)} \\ \vdots & \vdots & \ddots & \vdots \\ c_{(n+k)1} & c_{(n+k)2} & \cdots & 0 \end{bmatrix} \tag{25}$$

$$B = \begin{bmatrix} c_{11} & 0 & \cdots & 0 \\ 0 & c_{22} & \cdots & \vdots \\ \vdots & \vdots & \ddots & 0 \\ 0 & \cdots & 0 & c_{(n+k)(n+k)} \end{bmatrix} \tag{26}$$

According to the subadditivity of the normed linear space and the F norm definition, the following inequality can be obtained

$$\left\| \sum_{i=1}^{n+k} \sum_{j=1, j\neq i}^{n+k} |A_{ij}| + \sum_{i=1}^{n+k} |B_{ii}| \right\|_F \leq \left\| \sum_{i=1}^{n+k} \sum_{j=1, j\neq i}^{n+k} |A_{ij}| \right\|_F + \left\| \sum_{i=1}^{n+k} |B_{ii}| \right\|_F \tag{27}$$

The left-hand side of the inequality can be obtained as follows

$$\left\| \sum_{i=1}^{n+k} \sum_{j=1, j\neq i}^{n+k} |A_{ij}| + \sum_{i=1}^{n+k} |B_{ii}| \right\|_F = \left\| (C_N)^{-1} \right\|_F = \left(\sum_{i=1}^{n+k} \sum_{j=1}^{n+k} |C_{ij}|^2 \right)^{1/2}$$

$$= \left(trace\left((C_N)^{-T}(C_N)^{-1} \right) \right)^{1/2} = \left(\sum_{i=1}^{n+k} \lambda_i^2 \right)^{1/2} \tag{28}$$

where the index of the coupling characteristic of the must-pass points can be defined as follows
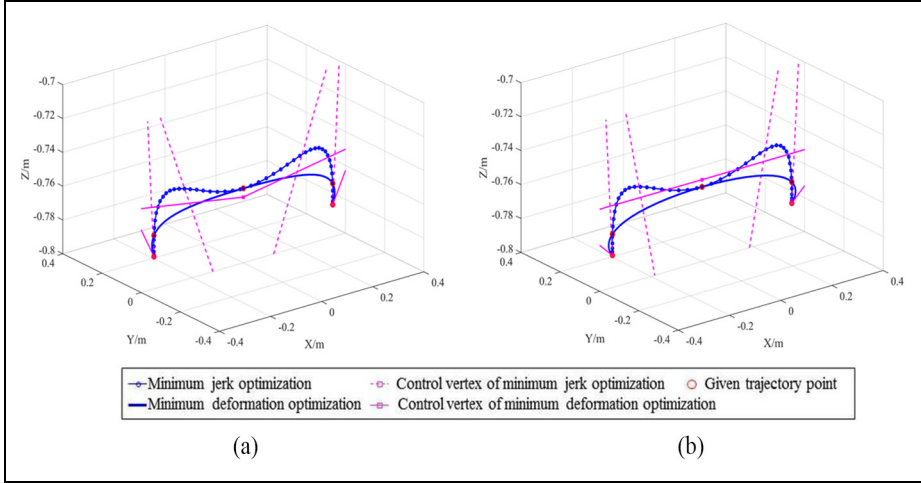
Figure 11. The motion trajectory after minimum jerk and deformation optimization: (a) the 5-time B-spline curve motion law and (b) the 7-time B-spline curve motion law.

$$\kappa_2 = \frac{\left[\left(\sum_{i=1}^{n+k} \lambda_i^2\right)^{1/2} - \left(\sum_{i=1}^{n+k} \sum_{j=1, j\neq i}^{n+k} \left|A_{ij}\right|^2\right)^{1/2}\right]}{\left(\sum_{i=1}^{n+k} \left|\lambda_i^2\right|^2\right)^{1/2}} \tag{29}$$

Then, according to the above constraint conditions of the optimization procedure, the minimum deformation index can be defined as follows

$$\kappa_{def} = min(\kappa_1, \kappa_2) \rightarrow min$$

$$s.t. \quad |C_{ii}| - \sum_{i=1}^{n+k} \sum_{j=1, j\neq i}^{n+k} |C_{ij}| > 0 \tag{30}$$

Then combining with constraint situation in equation (19), the minimum deformation optimization result is shown in Figure 11 and Table 6. After the minimum deformation optimization, the deformation distance of the trajectory is significantly lower than that of the trajectory after the minimum jerk optimization, and the control vertex of the former is closer to the given trajectory point, while the control vertex of the minimum jerk optimization is far from the given trajectory point. However, after the minimum deformation optimization, all the motion parameters of the robot joints are much higher than the value of minimum jerk optimization, especially in aspects of maximum jerkiness and maximum input torque of the robot joint. Therefore, in the process of the trajectory optimization, the minimum deformation and smoothness of the robot should be taken into account at the same time.

Table 6. The motion parameters of the robot joint with minimum deformation optimization.

	Motion law	T_1 (s)	T_2 (s)	max $|v|$ (°/s)	max $|a|$ (°/s²)	max $|j|$ (°/s³)	max $|\tau|$ (N m)
Optimization with minimum deformation	5-time B-spline	0.054	0.071	2.53×10^3	1.79×10^5	1.12×10^7	78.19
	7-time B-spline	0.070	0.055	3.22×10^3	3.28×10^5	2.45×10^7	132.97

Table 7. The motion parameters of the robot joint with the comprehensive index.

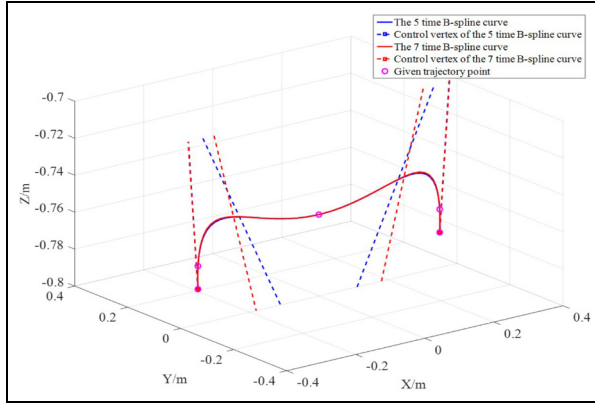|	Motion law	T_1 (s)	T_2 (a)	max $|v|$ (°/s)	max $|a|$ (°/s²)	max $|j|$ (°/s³)	max $|\tau|$ (N m)
Optimization with the comprehensive index	5-time B-spline	0.029	0.096	1.75×10^3	7.80×10^4	4.93×10^6	36.28
	7-time B-spline	0.038	0.087	1.93×10^3	7.81×10^4	3.98×10^6	40.15

Figure 12. The motion trajectory after comprehensive optimization.

According to the above analysis, combining with the two optimization indices of minimum jerk and minimum deformation, the new optimization index can be redefined as

$$\kappa_{jc} = \sqrt{\left(\kappa_{jerk}\right)^2 + \left(\xi_{def}\kappa_{def}\right)^2} \tag{31}$$

where ξ_{def} is the index weight of κ_{def} relative to κ_{jerk}, and according to the above optimization analysis result, the initial value of ξ_{def} is set to 1×10^5. So combining with the above constraint situations in equation (19), the final optimization model can be illustrated as follows

$$\kappa_{jc} \rightarrow \min \tag{32}$$

The optimization trajectory and motion parameter results are shown in Figure 12 and Table 7. It shows that although the comprehensive index optimization method simultaneously reduces the trajectory deformation and all motion parameters of the robot joint, the trajectory deformation distance still has a large deviation.

Hence, it needs to establish an error indictor κ_z to represent the minimum deviation between the maximum points of the optimized trajectory and setting trajectory on the z axis and to analyze the relation between $\kappa_{\Delta z}$, $max|j|$, and ξ_{def} to confirm a optimal value of ξ_{def}. Hence, the optimization model can be defined as follows

$$\exists \xi_{def}$$
$$s.t. \quad max|j| \rightarrow \min \quad |\kappa_{\Delta z}| \rightarrow \min$$

The calculation results are shown in Table 8, and it can be seen that as ξ_{def} increases, the error $\kappa_{\Delta z}$ of the 5- and 7-time B-spline curve shows a trend of gradual decrease. However, the value of $max|j|$ keeps increasing, especially in the 7-time B-spline curve, and its growth rate is most remarkable. In order to prevent the jerk over the big, and on the basis of fully taking the allowable deformability into

Table 8. The relation between $\kappa_{\Delta z}$, $max|j|$, and ξ_{def}.

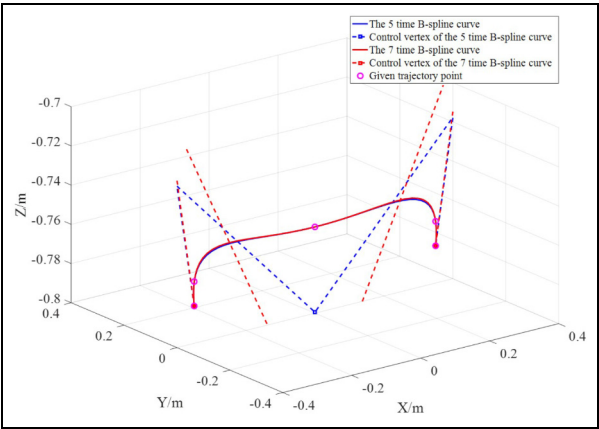| ξ_{def} 1×10^5	5-time B-spline		7-time B-spline	
	$max|j|$ (°/s³)	$\kappa_{\Delta z}$ (mm)	$max|j|$ (°/s³)	$\kappa_{\Delta z}$ (mm)
1	4.93×10^6	10	3.98×10^6	10
2	4.35×10^6	7.7	3.96×10^6	7.9
3	4.08×10^6	6.7	4.09×10^6	5.9
4	4.25×10^6	5.0	4.51×10^6	4.2
5	4.57×10^6	3.6	5.13×10^6	2.9
6	4.99×10^6	2.4	5.84×10^6	1.8
7	5.53×10^6	1.6	6.63×10^6	1.0
8	6.15×10^6	0.9	7.47×10^6	0.5
9	6.50×10^6	0.6	7.90×10^6	0.3
10	6.87×10^6	0.4	8.34×10^6	0.1

Figure 13. The motion trajectory with the optimum ξ_{def}.

account, it needs to try to reduce the value of robot joint. Therefore, the optimum value of the index weight ξ_{def} is set to 6×10^5 with 5-time B-spline curve and 5×10^5 with the 7-time B-spline curve. The trajectory simulation result is shown in Figure 13. Finally, the optimized robot joint jerk value is reduced by 69.4% and 72.3%, respectively, compared with that before the optimization, so the optimization process of this method is effective.

Conclusion

This article introduces a kind of 6-DOF high-speed parallel robot and analyzes its kinematic and dynamic problem. Then combining with its commonly used trajectory in industrial production line, it proposed the trajectory planning method in

operation space to achieve the smoothness and accuracy motion of the robot end-effector, so the conclusion can be summarized as follows:

1. Because of the non-liner mapping relationship existing in the process of the kinematic forward solution, the B-spline curve motion law is not suitable for trajectory planning in the joint space. It may cause the trajectory curve to deform, especially when the robot end-effector generates rotation motion.

2. For the trajectory planning in the operation space, the generated motion trajectory can be strictly followed to set the track requirements without deformation, especially the robot end-effector has rotation motion. Through comparison, it can be found that the 5- and 7-time B-spline curve can guarantee that no sharp points occur in the curve of each motion parameters of the robot joints, which is more suitable for 6-DOF high-speed parallel robot than the 3-time B-spline curve.

3. In the trajectory optimum produce, three optimization methods are analyzed. The minimum joint jerk optimization method can reduce the robot joint jerk by a wide margin, but the trajectory deformation error of the robot increases, which leads to uncontrollable motion of the robot. The minimum trajectory deformation optimization method has the opposite effect. Therefore, a comprehensive optimization method with a minimum joint jerk and trajectory deformation error is presented. Compared to without the optimization, the maximum robot joint jerk decreases by 69.4% and 72.3%, respectively, and the maximum torque decreases by 51.4% and 38.9%, respectively, under a suitable trajectory deformation.

Therefore, this method can improve the stability and smoothness of the robot motion, thereby suppressing the residual vibration. In future work, the space curve trajectory planning method will be further studied to find a curve optimization design method more suitable for the 6-DOF parallel robot.

Declaration of conflicting interests

Funding

ORCID iDs

Jiangping Mei ⓘ https://orcid.org/0000-0001-5261-8759
Fan Zhang ⓘ https://orcid.org/0000-0002-4913-2464

References

1. Korayem MH, Irani M and Nekoo SR. Load maximization of flexible joint mechanical manipulator using nonlinear optimal controller. *Acta Astronaut* 2011; 69(7–8): 458–469.
2. Korayem MH, Esfeden RA and Nekoo SR. Path planning algorithm in wheeled mobile manipulators based on motion of Arms. *J Mech Sci Tech* 2015; 29(4): 1753–1763.
3. Korayem MH, Nikoobin A and Azimi V. Maximum load carrying capacity of mobile manipulators: optimal control approach. *Robotica* 2009; 27(1): 147–159.
4. Zha XF. Optimal pose trajectory planning for robot manipulators. *Mech Machine Theory* 2002; 37(10): 1063–1086.
5. Tan G and Wang Y. Theoretical and experimental research on time-optimal trajectory planning and control of industrial robots. *Contr Theory Applicat* 2003; 20(2): 185–192.
6. Hervé JM. The Lie group of rigid body displacements, a fundamental tool for mechanism design. *Mech Mach Theory* 1999; 34: 719–730.
7. Bazaz SA and Tondu B. 3-cubic spline for online Cartesian space trajectory planning of an industrial manipulator. In: *Proceedings of the international workshop on advanced motion control*, Coimbra, 29 June–1 July 1998, pp. 493–498. New York: IEEE.
8. Gasparetto A and Zanotto V. A technique for time-jerk optimal planning of robot trajectories. *Robot Comp Integr Manufact* 2008; 24(3): 415–426.
9. Kaikai J. *Research on control method of high-speed parallel manipulators*. Tianjin, China: Tianjin University, 2014, pp. 20–33.
10. Zhengyu Q. *Dynamics model based research on control methods of high-speed parallel manipulators*. Tianjin, China: Tianjin University, 2015, pp. 27–39.
11. Angeles J, Rojas A and Lopez-Cajun CS. Trajectory planning in robotic continuous-path applications. *Robotics* 1988; 4(4): 380–385.
12. Macfarlane S and Croft E. Jerk-bounded manipulator trajectory planning design for real-time application. *IEEE Trans Robot Automat* 2003; 19(1): 42–52.
13. Liu SG, Zhu SQ and Wu WZ. Smoothness-optimal trajectory planning method with constraint on traveling time for manipulators. *Electr Mach Contr* 2010; 13(6): 897–902.
14. Li HZ, Le MD, Gong ZM, et al. Motion profile design to reduce residual vibration of high-speed positioning stages. *IEEE/ASME Trans Mechatr* 2009; 14(2): 264–269.
15. Sencer B, Altintas Y and Croft E. Feed optimization for five-axis CNC machine tools with drive constraints. *Int J Mach Tools Manufact* 2008; 48(7–8): 733–745.
16. Rew KH and Kim KS. Using asymmetric S-curve profile for fast and vibration-less motion. In: *Proceedings of the international conference on control, automation and systems*, Seoul, South Korea, 17–20 October 2007, pp. 500–504. New York: IEEE.
17. Ha CW, Rew KH and Kim KS. A complete solution to asymmetric S-curve motion profile: theory & experiments. In: *Proceedings of the international conference on control, automation and systems*, Seoul, South Korea, 14–17 October 2008, pp. 2845–2849. New York: IEEE.
18. Liu S. *Research on motion planning and trajectory tracking control of six-DOF serial robots*. Hangzhou, China: Zhejiang University, 2009, pp. 40–73.
19. Mei J, Zang J, Qiao Z, et al. Trajectory planning of 3-DOF delta parallel manipulator. *J Mech Eng* 2014; 50(6): 1–9.
20. Lin S, Liu X and Ou Y. The study of trajectory planning of manipulator in Cartesian space. *Mach Design Manufact* 2013; 3: 49–52.
21. Zhang LM, Mei J-P, Zhao X-M, et al. Dynamic dimensional synthesis of Delta robot. *J Mech Eng* 2010; 46(3): 1–7.

22. Piegl L and Tiller W. *The nurbs*. Berlin; Heidelberg: Springer; 1997.
23. Li Y, Huang T and Chetwynd DG. An approach for smooth trajectory planning of high-speed pick-and-place parallel robots using quintic B-splines. *Mech Machine Theory* 2018; 126: 479–490.
24. Shao Z-F, Tang X, Chen X, et al. Research on the inertia matching of the Stewart parallel manipulator. *Robot Comp Integr Manufact* 2012; 28(6): 649–659.

Author biographies

Jiangping Mei is professor, doctoral supervisor of the School of Mechanical and Engineering, Tianjin University, Tianjin, China. His main research direction is robot control and automation production line.

Fan Zhang is a Ph.D candidate of the School of Mechanical and Engineering, Tianjin University. His research interests include robot structure design, motion control and industrial production line applications.

Jiawei Zang is a Ph.D of Nanjing Estun co. LTD. His main direction is robot control system design.

Yanqin Zhao is a Ph.D candidate of the School of Mechanical and Engineering, Tianjin University, Tianjin, China. Her research interests are robot stiffness design.

Han Yan is a graduate student of the School of Mechanical and Engineering, Tianjin University. His research interests are robot control system design.